arXiv:2110.04375v1 [cs.LG] 8 Oct 2021

Neural Link Prediction with Walk Pooling

Liming Pan[1,*], Cheng Shi[2,*], and Ivan Dokmanić[2,3,†]

[1]School of Computer and Electronic Information, Nanjing Normal University
[2]Department of Mathematics and Computer Science, University of Basel
[3]Department of Electrical and Computer Engineering, University of Illinois at Urbana-Champaign

May 29, 2022

Abstract

Graph neural networks achieve high accuracy in link prediction by jointly leveraging graph topology and node attributes. Topology, however, is represented indirectly; state-of-the-art methods based on subgraph classification label nodes with distance to the target link, so that, although topological information is present, it is tempered by pooling. This makes it challenging to leverage features like loops and motifs associated with network formation mechanisms. We propose a link prediction algorithm based on a new pooling scheme called WalkPool. WalkPool combines the expressivity of topological heuristics with the feature-learning ability of neural networks. It summarizes a putative link by random walk probabilities of adjacent paths. Instead of extracting transition probabilities from the original graph, it computes the transition matrix of a "predictive" latent graph by applying attention to learned features; this may be interpreted as feature-sensitive topology fingerprinting. WalkPool can leverage unsupervised node features or be combined with GNNs and trained end-to-end. It outperforms state-of-the-art methods on all common link prediction benchmarks, both homophilic and heterophilic, with and without node attributes. Applying WalkPool to a set of unsupervised GNNs significantly improves prediction accuracy, suggesting that it may be used as a general-purpose graph pooling scheme.

∗ The first two authors have equal contribution.

† To whom correspondence should be addressed. Email: ivan.dokmanic@unibas.ch.

1 Introduction

Graphs are a natural model for relational data such as coauthorship networks or the human protein interactome. Since real-world graphs are often only partially observed, a central problem across all scientific domains is to predict missing links (Liben-Nowell & Kleinberg, 2007). Link prediction finds applications in predicting protein interactions (Qi et al., 2006), drug responses (Stanfield et al., 2017), or completing the knowledge graph (Nickel et al., 2015). It underpins recommender systems in social networks (Adamic & Adar, 2003) and online marketplaces (Lü et al., 2012). Successful link prediction demands an understanding of the principles behind graph formation.

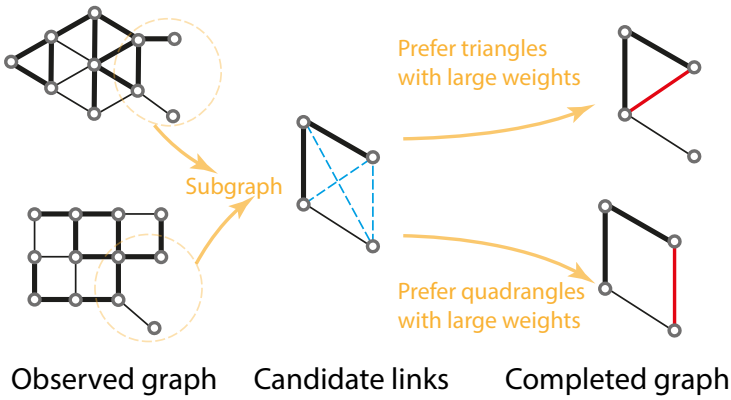

Figure 1: WalkPool "fingerprints" graph neighborhoods by reinterpreting attention coefficients as random walk probabilities and thus making heuristics trainable.

In this paper we propose a link prediction algorithm which builds on two distinct traditions: (1) complex networks, from which we borrow ideas about importance of topology, and (2) the emerging domain of graph neural networks (GNNs), on which we rely to learn optimal features. The central part of our algorithm is a new random-walk-based pooling mechanism called WalkPool which may be interepreted as a learnable version of topological heuristics (Figure 1). Our algorithm is universal in the sense of Chien et al. (2020) in that it models both heterophilic and homophilic graphs unlike hardcoded heuristics or standard GNNs which work better on homophilic graphs. WalkPool achieves state-of-the-art link prediction results on all common benchmark datasets, sometimes by a significant margin, even on datasets like **USAir** (Batagelj & Mrvar, 2006) where the previous state of the art is as high as 97%.

1.1 Related work

Early studies on link prediction use heuristics from social network analysis (Lü & Zhou, 2011). The homophily mechanism for example (McPherson et al., 2001) asserts that "similar" nodes connect. Most heuristics are based on connectivity: the common-neighbor index (CN) scores a pair of nodes by the number of shared neighbors, yielding predicted graphs with many triangles; Adamić–Adar index (AA) assumes that a highly-connected neighbor contributes less to the score of a focal link (Adamic & Adar, 2003). CN and AA rely on paths of length two. Others heuristics use longer paths, explicitly accounting for long-range correlations (Lü & Zhou, 2011). The Katz index (Katz, 1953) scores a pair of nodes by a weighted sum of the number of walks of all possible lengths. PageRank scores a link by the probability that a walker starting at one end of the link reaches the other in the stationary state under a random walk model with restarts.

Heuristics make strong assumptions such as a particular parametric decay of path weights with length, often tailored to either homophilic or heterophilic graphs. Moreover, they cannot be easily used on graphs with node or edge features. Instead of hard-coded structural features, link prediction algorithms based on GNNs like the VGAE (Kipf & Welling, 2016b) or SEAL Zhang & Chen (2018) use learned node-level representations that capture both the structure and the features, yielding unprecedented accuracy.

Two strategies have proved successful for GNN-based link prediction. The first is to devise a score function which only depends on the two nodes that define a link. The second is to extract a

subgraph around the focal link and solve link prediction by (sub)graph classification (Wu et al., 2020). In both cases the node representations are either learned in an unsupervised way (Kipf & Welling, 2016b; Mavromatis & Karypis, 2020) or computed by a GNN trained joinly with the link classifier (Zhang & Chen, 2018; Zhang et al., 2020).

Algorithms based on two-body score functions achieved state-of-the-art performance when they appeared, but real networks brim with many-body correlations. Graphs in biochemistry, neurobiology, ecology, and engineering (Milo et al., 2004) exhibit *motifs*—distinct patterns occuring much more often than in random graphs. Motifs may correspond to basic computational elements and relate to function (Shen-Orr et al., 2002). A multilayer GNN generates node representation by aggregating information from neighbors, capturing to some extent many-body and long-range correlations. This dependence is however indirect and complex topological properties such as frequency of motifs are smoothed out.

The current state-of-the-art link prediction algorithm, SEAL (Zhang & Chen, 2018), is based on subgraph classification and thus may account for higher-order correlations. Unlike in vanilla graph classification where a priori all links are equaly important, in graph classification for link prediction the focal link plays a special role and the relative placement of other links with respect to it matters. SEAL takes this into account by labeling each node of the subgraph by its distance to the focal link. This endows the GNN with first-order topological information and helps distinguish relevant nodes in the pooled representation. Zhang and Chen show that node labeling is essential for SEAL's exceptional accuracy. Nevertheless, important structural motifs are represented indirectly (if at all) by such labeling schemes, even less so after average pooling. We hypothesize that a major impediment to performance of link prediction comes from suboptimal pooling which fails to account for topology.

1.2 Our contribution

Following Zhang & Chen (2018), we approach link prediction from the perspective of subgraph classification. Instead of encoding relative topological information through node labels, we design a new pooling mechanism we call WalkPool. WalkPool extracts higher-order structural information by encoding node representations and graph topolgy into random-walk transition probabilities on some effective *latent* graph, and then using those probabilities to compute features we call *walk profiles*. WalkPool generalizes loop-counting ideas used to build expressive graph models (Pan et al., 2016).

Using normalized probabilities tuned by graph attention mitigates the well-known issue in graph learning that highly-connected nodes may bias predictions. Transition probabilities and the derived walk profiles have simple topological interpretations.

WalkPool can be applied to node representations generated by any unsupervised graph representation models or combined with GNNs and trained in an end-to-end fashion. We show that WalkPool achieves state-of-the-art results on all common link prediction benchmarks. Our code and data are available online at `https://github.com/DaDaCheng/WalkPooling`.

2 Link prediction on graphs

We consider an *observed* graph with N nodes (or vertices), $\mathcal{G}^o = (\mathcal{V}, \mathcal{E}^o)$, with $\mathcal{V}$ being the node set and $\mathcal{E}^o$ the set of *observed* links (or edges). The observed link set $\mathcal{E}^o$ is a subset $\mathcal{E}^o \subset \mathcal{E}^*$ of the set of all true links $\mathcal{E}^*$. The target of link prediction is to infer missing links from a candidate set $\mathcal{E}^c$, which contains both true (in $\mathcal{E}^*$) and false (not in $\mathcal{E}^*$) missing links.

Problem 1. *(Link prediction) Design an algorithm* `LearnLP` *that takes an observed graph* $\mathcal{G}^o \subset \mathcal{G}$ *and produces a link predictor* $\texttt{LearnLP}(\mathcal{G}^o) = \Pi \ : \ \mathcal{V} \times \mathcal{V} \to \{\text{True}, \text{False}\}$ *which accurately classifies links in* $\mathcal{E}^c$.

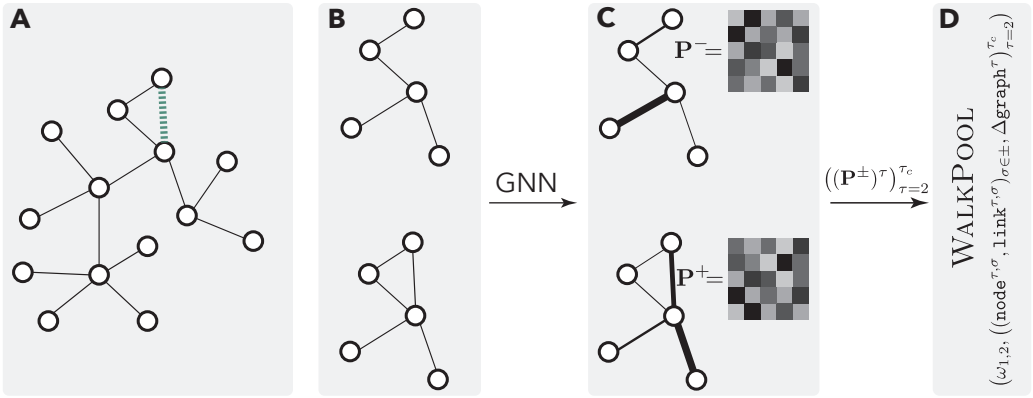

Figure 2: Illustration of WalkPool. **A**: The input graph and the focal link e; **B**: enclosing subgraphs with and without e; **C**: attention-processed features $\equiv$ random walk transition probabilities; **D**: extracted walk profile.

Well-performing solutions to Problem 1 exploit structural and functional regularities in the observed graph to make inferences about unobserved links.

Path counts and random walks For simplicity we identify the N vertices with integers $1, \ldots, N$ and represent $\mathcal{G}$ by its adjacency matrix, $\mathbf{A} = (a_{ij})_{i,j=1}^{N} \in \{0,1\}^{N\times N}$ with $a_{ij} = 1$ if $\{i,j\} \in \mathcal{E}^o$ and $a_{ij} = 0$ otherwise. Nodes may have associated feature vectors ($\mathbf{x}_i \in \mathbb{R}^F, i \in \{1, \ldots, N\}$); we collect all feature vectors in the feature matrix $\mathbf{X} = [\mathbf{x}_1, \cdots, \mathbf{x}_N]^T \in \mathbb{R}^{N\times F}$.

Integer powers of the adjacency matrix reveal structural information: $[\mathbf{A}^{\tau}]_{ij}$ is the number of paths of length τ connecting nodes i and j. WalkPool relies on random walk transition matrices. For an adjacency matrix $\mathbf{A}$ the transition matrix is defined as $\mathbf{P} = \mathbf{D}^{-1}\mathbf{A}$ where $\mathbf{D} = \mathrm{diag}(d_1, \ldots, d_N)$ and $d_i = \sum_j a_{ij} = |\mathcal{N}(i)|$ is the degree of the node i. Thus the probability $p_{ij} = d_i^{-1} a_{ij}$ that a random walker at node i transitions to node j is inversely proportional to the number of neighbors of i. An extension to graphs with non-negative edge weights $\mathbf{W} = (w_{ij})$ is straightforward by replacing a_{ij} by w_{ij}. Powers of $\mathbf{P}$ are interpretable: $[\mathbf{P}^{\tau}]_{ij}$ is the probability that a random walker starting at node i will reach node j in τ hops.

As we show in Section 3.2, transition probabilities in WalkPool are determined as coefficients of an attention mechanism applied to learned node features. The node features are in turn extracted by a parameterized function f_θ, which distills input attributes and to an extent graph topology into an embedding (a vector) for each node. The feature extractor $f_\theta : \{0,1\}^{N\times N} \times \mathbb{R}^{N\times F} \to \mathbb{R}^{N\times F'}$ takes as input the adjacency matrix (which encodes the graph topology) and the input feature matrix, and outputs a distilled node feature matrix. It should thus be equivariant to node ordering in $\mathbf{A}$ which is satisfied by GNNs.

3 WalkPool for link prediction by subgraph classification

We now describe WalkPool which directly leverages higher-order topological correlations without resorting to link labeling schemes and without making strong a priori assumptions. WalkPool first samples the k-hop subgraph $\mathcal{G}^k_{\{i,j\}} \subset \mathcal{G}^o$ enclosing the target link; and then computes random-walk profiles for sampled subgraphs with and without the target link. Random walk profiles are then fed into a link classifier.

Computing walk profiles entails

1. **Feature extraction**: $\mathbf{Z} = f_\theta(\mathbf{A}, \mathbf{X})$, where f_θ is a GNN;
2. **Transition matrix**: $\mathbf{P} = \mathtt{AttentionCoefficients}_\theta(\mathbf{Z}; \mathcal{G})$;

3. **Walk profiles**: Extract entries from $\mathbf{P}^\tau$ for $2 \leq \tau \leq \tau_c$ related to the focal link.

We emphasize that we do not use attention to compute per-node linear combinations of features like Veličković et al. (2017) (which is analogous to Vaswani et al. (2017)), but rather interpret the attention *coefficients* as random walk transition probabilities. The features $\mathbf{Z}$ may be obtained either by an unsupervised GNN such as VGAE (Kipf & Welling, 2016b), or they may be computed by a GNN which is trained jointly with WalkPool.

3.1 Sampling the enclosing subgraphs

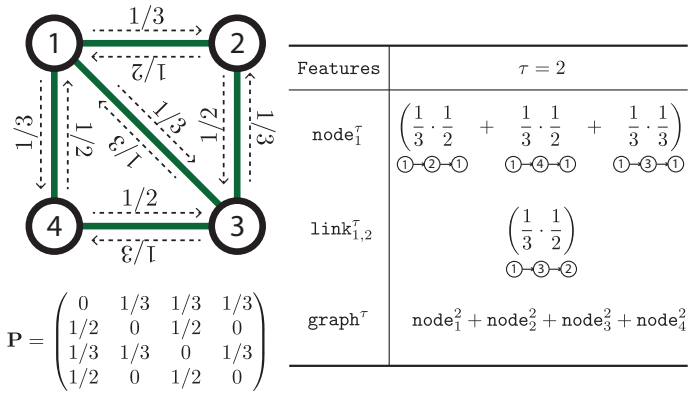

Figure 3: Illustration of features in walk profiles for $\tau = 2$. We assume $p_{i,j} = 1/d_i$ where d_i is the degree of node i.

Following earlier work we make the assumption that the presence of a link only depends on its neighbors within a (small) radius k. It is known that simple heuristics like AA may already perform well on many graphs, with longer walks not bringing about significant gains. Indeed, SEAL (Zhang & Chen, 2018) exploits the fact that an order k heuristic can be accurately calculated from a k-hop subgraph; optimal k is related to the underlying generative model. Keeping k small (as small as 2 in this paper) is pragmatic for reasons beyond diminishing returns: a large k greatly increases memory and compute demands. The size of a 2-hop neighborhood is graph-dependent, but for the highly-connected E.coli and PB datasets we already need to enforce a maximum number of nodes per hop to fit the subgraphs in memory.

Let $d(x, y)$ be the shortest-path distance between nodes x and y. The k-hop enclosing subgraph $\mathcal{G}^k_{\{i,j\}}$ for $\{i, j\}$ is defined as the subgraph induced from $\mathcal{G}^o$ by the set of nodes

$$\mathcal{V}^k_{\{i,j\}} = \{x \in \mathcal{V} \ : \ d(x, i) \leq k \text{ or } d(x, j) \leq k\}.$$

Then $\mathcal{G}^k_{\{i,j\}} = (\mathcal{V}^k_{\{i,j\}}, \mathcal{E}^k_{\{i,j\}})$, where $\{x, y\} \in \mathcal{E}^k_{i,j}$ when $x, y \in \mathcal{V}^k_{\{i,j\}}$ and $\{x, y\} \in \mathcal{E}^o$. We omit the dependence on k and write $G_{\{i,j\}} = (\mathcal{V}_{\{i,j\}}, \mathcal{E}_{\{i,j\}})$ for simplicity.

We fix an arbitrary order of the nodes in $\mathcal{V}_{\{i,j\}}$ and denote the corresponding adjacency matrix by $\mathbf{A}_{\{i,j\}}$. Without loss of generality, we assume that under the chosen order of nodes, the nodes i and j are labeled as 1 and 2 so that the candidate link $\{i, j\}$ is mapped to $\{1, 2\}$ in its enclosing subgraph. We denote the corresponding node feature matrix $\mathbf{Z}_{\{i,j\}}$, with values inherited from the full graph (the rows of $\mathbf{Z}_{\{i,j\}}$ are a subset of rows of $\mathbf{Z}$).

For the candidate set of links $\mathcal{E}^c$, we construct a set of enclosing subgraphs $\mathcal{S}^c = \{G_{\{i,j\}} : \{i, j\} \in \mathcal{E}^c\}$, thus transforming the link prediction problem into classifying these k-hop enclosing subgraphs. For training, we sample a set of edges $\mathcal{E}^t$ consisting of known positive and negative edges, and construct its corresponding enclosing subgraph set $\mathcal{S}^t = \{G_{i,j} : (i, j) \in \mathcal{E}^t\}$.

3.2 Random-walk profile

The next step is to classify the sampled subgraphs from their adjacency relations $\mathbf{A}_{\{i,j\}}$ and node representations $\mathbf{Z}_{\{i,j\}}$. Inspired by the walk-based heuristics, we employ random walks to infer higher-order topological information. Namely, for a subgraph $(\mathcal{G} = (\mathcal{V}, \mathcal{E}), \mathbf{Z})$ (either in $\mathcal{S}^c$ or $\mathcal{S}^t$) we encode the node representations $\mathbf{Z}$ into edge weights and use these edge weights

to compute transition probabilities of a random walk on the underlying graph. Probabilities of walks of various lengths under this model yield a *profile* of the focal link.

We first encode two-node correlations as

$$\omega_{x,y} = \frac{Q_\theta(\mathbf{z}_x)^T K_\theta(\mathbf{z}_y)}{\sqrt{F''}}, \tag{1}$$

for all $\{x, y\} \in \mathcal{E}$, where $Q_\theta : \mathbb{R}^{F'} \to \mathbb{R}^{F''}$ and $K_\theta : \mathbb{R}^{F'} \to \mathbb{R}^{F''}$ are two multilayer perceptrons (MLPs) and F'' is the output dimension of the MLPs. In order to include higher-order topological information, we compute the random-walk transition matrix $\mathbf{P} = (p_{x,y})$ from the two-body correlations

$$p_{x,y} = \begin{cases} \left[\text{softmax}\left((\omega_{x,z})_{z\in\mathcal{N}(x)}\right)\right]_y \equiv \dfrac{\exp(\omega_{x,y})}{\sum_{z\in\mathcal{N}(x)}\exp(\omega_{x,z})} & \text{if } \{x,y\} \in \mathcal{E} \\ 0 & \text{if } \{x,y\} \notin \mathcal{E} \end{cases} \tag{2}$$

where $\mathcal{N}(x)$ is the set of neighbors of x in the enclosing subgraph. The encoding function (2) has a form analogous to graph attention coefficients (Veličković et al., 2017; Shi et al., 2020); unlike graph attention, however, we directly use the coefficients instead of using them to compute linear combinations. We note in the passing that this framework also allows multi-head attention.

Entries of the τ-th power $[\mathbf{P}^\tau]_{ij}$ are interpreted as probabilities that a random walker goes from i to j in τ hops. These probabilities thus concentrate the topological *and* node attributes relevant for the focal link into the form of random-walks:

- Topology is included indirectly through the GNN-extracted node features $\mathbf{Z}$, and directly by the fact that $\mathbf{P}$ encodes zero probabilities for non-neighbors and that its powers thus encode probabilities of paths and loops;
- Input features are included directly through the GNN-extracted node features, and refined and combined with topology by the key and value functions Q_θ, K_θ.

As a result, WalkPool can be interpreted as trainable heuristics.

From the matrix $\mathbf{P}$ and its powers, we now read a list of features to be used in graph classification. We compute node-level, link-level, and graph-level features:

$$\texttt{node}^\tau = [\mathbf{P}^\tau]_{1,1} + [\mathbf{P}^\tau]_{2,2}, \qquad \texttt{link}^\tau = [\mathbf{P}^\tau]_{1,2} + [\mathbf{P}^\tau]_{2,1}, \qquad \texttt{graph}^\tau = \text{tr}[\mathbf{P}^\tau]. \tag{3}$$

Computation of all features is illustrated for $\tau = 2$ in Figure 3. Node-level features $\texttt{node}^\tau$ describe the loop structure around the candidate link (recall that $\{1, 2\}$ is the focal link in the subgraph). The summation ensures that the feature is invariant to the ordering of i and j, consistent with the fact that we study undirected graphs. Link-level features $\texttt{link}^\tau$ give the symmetrized probability that a length-τ random walk goes from node 1 to 2. Finally, graph-level features $\texttt{graph}^\tau$ are related to the total probability of length-τ loops. All features depend on the node representation $\mathbf{Z}$; we omit this dependence for simplicity.

3.3 Perturbation extraction

A true link is by definition always present in its enclosing subgraph while a negative link is always absent. This leads to overfitting if we directly compute the features (3) on the enclosing subgraphs since the presence or absence of the link has a strong effect on walk profiles. For a normalized comparison of true and false links, we adopt a perturbation approach. Given an enclosing subgraph $\mathcal{G} = (\mathcal{V}, \mathcal{E})$, we define its variants $\mathcal{G}^+ = (\mathcal{V}, \mathcal{E} \cup \{1, 2\})$ (resp. $\mathcal{G}^- = (\mathcal{V}, \mathcal{E}\backslash\{1, 2\})$) with the candidate link forced to be present (resp. absent). We denote the node-level features (3) computed on $\mathcal{G}^+$ and $\mathcal{G}^-$ by $\texttt{node}^{\tau,+}$ and $\texttt{node}^{\tau,-}$, respectively, and analogously for the link- and graph-level features.

While the node- and link-level features are similar to the heuristics of counting walks, $\texttt{graph}^{\tau,+}$ and $\texttt{graph}^{\tau,-}$ are not directly useful for link prediction as discussed in the introduction: the information related to the presence of $\{i, j\}$ is obfuscated by the summation over the entire subgraph (by taking the trace).

SEAL attempts to remedy a similar issue for average (as opposed to $\mathrm{tr}(\mathbf{P}^\tau)$) pooling by labeling nodes by distance from the link. Here we propose a principled alternative. Since transition probabilities are normalized and have clear topological meaning, we can suppress irrelevant information by measuring the perturbation of graph-level features,

$$\Delta\texttt{graph}^\tau = \texttt{graph}^{\tau,+} - \texttt{graph}^{\tau,-}. \tag{4}$$

This "background subtraction" induces a data-driven soft limit on the longest loop length so that, by design, $\Delta\texttt{graph}^\tau$ concentrates around the focal link. In Appendix D, we demonstrate locality of WalkPool.

Compared to node labeling, the perturbation approach does not manually assign a relative position (which may wrongly suggest that nodes at the same distance from the candidate link are of equal importance).

In summary, with WalkPool, for all $\mathcal{G} \in \{\mathcal{G}_{\{i,j\}} : \{i, j\} \in \mathcal{E}^c\}$, we read a list of features as

$$\texttt{WP}_\theta(G, \mathbf{Z}) = \left[\omega_{1,2}, \left(\texttt{node}^{\tau,+}, \texttt{node}^{\tau,-}, \texttt{link}^{\tau,+}, \texttt{link}^{\tau,-}, \Delta\texttt{graph}^\tau\right)_{\tau=2}^{\tau_c}\right], \tag{5}$$

where τ_c is the cutoff of the walk length and we treat it as a hyperparameter. The features are finally fed into a classifier; we use an MLP Π_θ with a sigmoid activation in the output. The ablation study in Table 3 (Appendix A) shows that all the computed features contribute relevant predictive information. Walk profile computation is summarized in Figure 2.

3.4 Training the model

The described model depends on trainable parameters θ. These parameters are fitted on the given observed set $\mathcal{E}^t$ of positive and negative training links and their enclosing subgraphs. We perform WalkPool for each subgraph and minimize the MSE loss (with a sigmoid in the last layer of the classifier MLP Π_θ),

$$\theta^* = \arg\min_\theta \frac{1}{|\mathcal{E}^t|} \sum_{\{i,j\}\in\mathcal{E}^t} \left(y_{\{i,j\}} - \Pi_\theta\left(\texttt{WP}_\theta(\mathcal{G}_{\{i,j\}}, \mathbf{Z}_{\{i,j\}})\right)\right)^2$$

where $y_{\{i,j\}} = 1$ if $\{i, j\} \in \mathcal{E}^o$ and 0 otherwise is the label indicating whether the link $\{i, j\}$ is true or false. The fitted model is then deployed on the candidate links $\mathcal{E}^c$; the predicted label for $\{x, y\} \in \mathcal{E}^c$ is simply $\widehat{y}_{\{x,y\}} = \Pi_{\theta^*}(\texttt{WP}_{\theta^*}(\mathcal{G}_{\{x,y\}}), \mathbf{Z}_{\{x,y\}})$.

4 Performance of WalkPool on benchmark datasets

In this section, we describe extensive experiments we conducted to evaluate WalkPool. We use area under the curve (AUC) (Bradley, 1997) and average precision (AP) as evaluation metrics. Precision is defined as the fraction of true positives among the predicted links. Letting TP (FP) be the number of true (false) positive links, $\mathrm{AP} = \mathrm{TP}/(\mathrm{TP} + \mathrm{FP})$.

4.1 Datasets

In homophilic (heterophilic) graphs, nodes that are similar (dissimilar) are more likely to connect. For node classification, a homophily index is defined formally as the average fraction of neighbors with identical labels (Pei et al., 2020). In the context of link prediction, if we assume that network

formation is driven by the similarity (or dissimilarity) of node attributes, then a homophilic graph will favor triangles while a heterophilic graph will inhibit triangles. Following this intuition, we adopt the average clustering coefficient ACC (Watts & Strogatz, 1998) as a topological correlate of homophily.

We consider eight datasets without input node attributes and three with node attributes. The ones without features are:

- **USAir** (Batagelj & Mrvar, 2006): a graph of US airlines with 332 nodes and 2126 edges; $\texttt{ACC} = 0.625$.
- **NS** (Newman, 2006): the collaboration relation of network science researchers with 1589 nodes and 2742 edges; $\texttt{ACC} = 0.638$.
- **PB** (Ackland et al., 2005): a graph of hyperlinks between weblogs on US politics with 1222 nodes and 16714 edges; $\texttt{ACC} = 0.320$.
- **Yeast** (Von Mering et al., 2002): a protein-protein interaction graph in yeast with 2375 nodes and 11693 edges; $\texttt{ACC} = 0.306$.
- **C.ele** (Watts & Strogatz, 1998): the biological neural network of C.elegans with 297 nodes and 2148 edges; $\texttt{ACC} = 0.292$.
- **Power** (Watts & Strogatz, 1998): the topology of the Western States Power Grid of the United States with 4941 nodes and 6594 edges; $\texttt{ACC} = 0.080$.
- **Router** (Spring et al., 2002): the router-level Internet with 5022 nodes and 6258 edges; $\texttt{ACC} = 0.012$.
- **E.coli** (Zhang et al., 2018): the pairwise reaction relation of metabolites in E.coli with 1805 nodes and 15660 edges; $\texttt{ACC} = 0.516$.

In graphs with very low average clustering coefficient like **Power** and **Router**, topology-based heuristics usually perform poorly (Lü & Zhou, 2011) (cf. Table 1), since heuristics often adopt the homophily assumption and rely on triangles. We show that by *learning* the topological organizing patterns, WalkPool performs well even for these graphs.

For a fair comparison, we use the exact same training and testing sets (including positive and negative links) as SEAL in Zhang & Chen (2018), as provided by the authors. In particular, 90% of edges are taken as training positive edges and the remaining 10% are the positive test edges. The same number of additionally sampled nonexistent links are taken as training and testing negative edges.

As graphs *with* node attributes, we consider three citation graphs with publications described by binary vectors indicating the absence/presence of the corresponding dictionary word.

- **Cora** (McCallum et al., 2000): a citation graph with 2708 scientific publications and 5429 links. The dictionary consists of 1433 unique words; $\texttt{ACC} = 0.241$.
- **Citeseer** (Giles et al., 1998): the dataset consists of 3312 scientific publications with 4732 links; the dictionary consists of 3703 unique words; $\texttt{ACC} = 0.141$.
- **Pubmed** (Namata et al., 2012): the dataset consists of 19717 scientific publications with 44338 links. The dictionary consists of 500 unique words; $\texttt{ACC} = 0.060$.

Following the experimental protocols in (Kipf & Welling, 2016b; Pan et al., 2018; Mavromatis & Karypis, 2020), we split the links in three parts: 10% testing, 5% validation, 85% training. We sample the same number of nonexisting links in each group as negative links.

4.2 Baselines

On benchmarks without node attributes, we compare WalkPool with eight other methods. We consider three walk-based heuristics: AA, Katz and PR; two subgraph-based heuristic learning methods: Weisfeiler–Lehman graph kernel (WLK) (Shervashidze et al., 2011) and WLNM (Zhang & Chen, 2017); and latent feature methods: node2vec (N2V) (Grover & Leskovec, 2016) and spectral clustering (SPC) (Tang & Liu, 2011). We additionally consider the GNN-based SEAL, which is the previous state-of-the-art.

For datasets with node attributes, we combine WalkPool with three unsupervised GNN-based models: the VGAE, adversarially regularized variational graph autoencoder (ARGVA) (Pan et al., 2018) and Graph InfoClust (GIC) (Mavromatis & Karypis, 2020).

4.3 Implementation details

In the absence of node attributes, we initialize the node representation $\mathbf{Z}^{(0)}$ as an $N \times F^{(0)}$ all-ones matrix, with $F^{(0)} = 32$. We generate node representations by a two-layered Graph Convolutional Network (GCN) (Kipf & Welling, 2016a): $\mathbf{Z}^{(k)} = \mathrm{GCN}\left(\mathbf{Z}^{(k-1)}\right), k \in \{1, 2\}$, where $\mathbf{Z}^{(0)} = \mathbf{X}$. We then concatenate the outputs as $\mathbf{Z} = [\mathbf{Z}^{(0)} \mid \mathbf{Z}^{(1)} \mid \mathbf{Z}^{(2)}]$ to obtain the final node representation used to compute $\mathtt{WP}(G, \mathbf{Z})$ and classify. While a node labeling scheme like the one in SEAL is not needed for the strong perfomance of WalkPool, we find that labeling nodes by distance to focal link slightly improves results; we thus evaluate WalkPool with and without distance labels (DL).

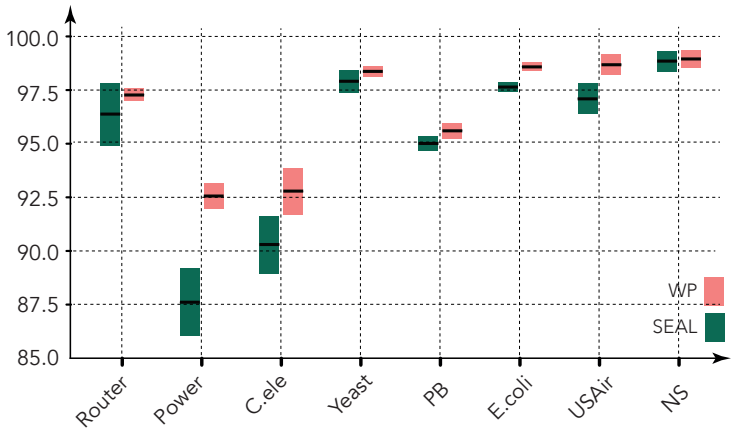

Figure 4: Comparison of mean and variance of AUC between SEAL and WP with 90% observed links. The datasets are sorted by their clustering coefficients. From left to right: Router(0.012), Power(0.080), C.ele(0.292), Yeast(0.306), PB(0.320), E.coli(0.516), USAir(0.625), NS(0.638).

For the three datasets with node attributes, we first adopt an unsupervised model to generate an initial node representation $\mathbf{Z}^{(0)}$. This is because standard 2-layer GCNs are not expressive enough to extract useful node features in the presence of node attributes Zhang et al. (2019).

The initial node representation is fed into the same two-layered GCN above, and we take the concatenated representation $\mathbf{Z} = [\mathbf{Z}^{(0)} \mid \mathbf{Z}^{(1)} \mid \mathbf{Z}^{(2)}]$ as the input to WalkPool. The hyperparameters of the model are explained in detail in Appendix B.

4.4 Results

Datasets without attributes We perform 10 random splits of the data. The average AUCs with standard deviations are shown in Table 1; the AP results can be found in Appendix C. For WalkPool, we have considered both the cases with and without the DL node labels as input features.

From Table 1, WalkPool significantly improves the prediction accuracy on all the datasets we have considered. It also has a smaller standard deviation, indicating that WalkPool is stable on independent data splits (unlike competing learning methods). Among all methods, WalkPool with DL performs the best; the second-best method slightly below is WalkPool without DL.

Data	USAir	NS	PB	Yeast	C.ele	Power	Router	E.coli
AA	95.06±1.03	94.45±0.93	92.36±0.34	89.43±0.62	86.95±1.40	58.79±0.88	56.43±0.51	95.36±0.34
Katz	92.88±1.42	94.85±1.10	92.92±0.35	92.24±0.61	86.34±1.89	65.39±1.59	38.62±1.35	93.50±0.44
PR	94.67±1.08	94.89±1.08	93.54±0.41	92.76±0.55	90.32±1.49	66.00±1.59	38.76±1.39	95.57±0.44
WLK	96.63±0.73	98.57±0.51	93.83±0.59	95.86±0.54	89.72±1.67	82.41±3.43	87.42±2.08	96.94±0.29
WLNM	95.95±1.10	98.61±0.49	93.49±0.47	95.62±0.52	86.18±1.72	84.76±0.98	94.41±0.88	97.21±0.27
N2V	91.44±1.78	91.52±1.28	85.79±0.78	93.67±0.46	84.11±1.27	76.22±0.92	65.46±0.86	90.82±1.49
SPC	74.22±3.11	89.94±2.39	83.96±0.86	93.25±0.40	51.90±2.57	91.78±0.61	68.79±2.42	94.92±0.32
SEAL	97.09±0.70	98.85±0.47	95.01±0.34	97.91±0.52	90.30±1.35	87.61±1.57	96.38±1.45	97.64±0.22
WP(ones)	98.52±0.50	98.86±0.42	95.42±0.39	98.16±0.33	92.42±1.22	91.71±0.60	97.18±0.28	98.54±0.20
WP(DL)	**98.68±0.48**	**98.95±0.41**	**95.60±0.37**	**98.37±0.25**	**92.79±1.09**	**92.56±0.60**	**97.27±0.28**	**98.58±0.19**

Table 1: Prediction accuracy measured by AUC on eight datasets (90% observed links) without node attributes. Boldface marks the best, underline the second best results.

	VGAE		ARGVA		GIC	
	NO WP	WP	NO WP	WP	NO WP	WP
Cora	91.98±0.54	94.64±0.55	92.45±1.11	94.71±0.85	93.68±0.59	**95.90±0.50**
Citeseer	91.21±1.14	94.32±0.90	91.71±1.38	94.53±1.77	95.03±0.65	**95.94±0.53**
Pubmed	96.51±0.14	98.49±0.13	96.62±0.12	98.52±0.14	93.00±0.36	**98.72±0.10**

Table 2: Prediction accuracy measured by AUC on three datasets (90% observed links) with node attributes.

We find that WalkPool performs stably on both homophilic (high average clustering) and heterophilic (low average clustering) datasets, achieving state-of-the-art performance on all. Remarkably, on **Power** and **Router** where topology-based heuristics such as AA and Katz fail, WalkPool shows strong performance (it also outperforms SEAL by about 5% on **Power**). This confirms that walk profiles are expressive descriptors of the local network organizing patterns, and that WalkPool can fit their parameters from data without making prior topological assumptions.

Datasets with node attributes We apply WalkPool to extract higher-order information from node representations generated via unsupervised learning. We again perform 10 random splits of the data and report the average AUC with standard deviations in Table 2; for AP see Appendix D. In Table 2, we show the results of unsupervised models with and without WalkPool. For all the unsupervised models and datasets, WalkPool improves the prediction accuracy. On the **Pubmed** dataset where the relative importance of topology over features is greater, WalkPool brings about the most significant gains.

While traditional heuristics cannot include node attributes, WalkPool encodes the node attributes into random walk transition probabilities via the attention mechanism, which allows it to capture structure and node attributes simultaneously. The prediction accuracy relies on the unsupervised GNN which generates the inital node representation. We find that the combination of GIC and WalkPool yields the highest accuracy for all three datasets. Importance of initial node representations is plain since WalkPool is not designed to uncover structure in node attributes. Nonetheless, WalkPool greatly improves performance of unsupervised GNN on the downstream link prediction task.

5 Discussion

Link prediction differs from node classification in that the topology of the underlying graph plays an essential role, even with node attributes present. Link prediction and topology are entangled, so to speak, since topology is *defined* by the links. Most GNN-based link prediction

methods generate predictions from node representations and thus do not adequately leverage topological information.

Our proposed WalkPool, to the contrary, jointly encodes node representations and graph topology into *learned* topological features. The central idea is how to leverage learning: we apply attention to the node representations and interpret the attention coefficients as transition probabilities of a graph random walk. WalkPool is a trainable topological heuristic, thus explicitly considering long-range correlations, but without making ad hoc assumptions like the classical heuristics.

This intuition is borne out in practice: combining supervised or unsupervised graph neural networks with WalkPool yields state-of-the-art performance on a broad range of benchmarks with diverse structural characteristics. Remarkably, WalkPool achieves this with the same set of hyperparameters on all tasks regardless of the network type and generating mechanism.

Acknowledgments

LP would like to acknowledge support from National Natural Science Foundation of China under Grand No. 62006122. CS and ID were supported by the European Research Council (ERC) Starting Grant 852821—SWING.

References

Robert Ackland et al. Mapping the us political blogosphere: Are conservative bloggers more prominent? In *BlogTalk Downunder 2005 Conference, Sydney*, 2005.

Lada A Adamic and Eytan Adar. Friends and neighbors on the web. *Social networks*, 25(3): 211–230, 2003.

Vladimir Batagelj and Andrej Mrvar. Pajek datasets website. `http://vlado.fmf.uni-lj.si/pub/networks/data/`, 2006.

Andrew P Bradley. The use of the area under the roc curve in the evaluation of machine learning algorithms. *Pattern recognition*, 30(7):1145–1159, 1997.

Eli Chien, Jianhao Peng, Pan Li, and Olgica Milenkovic. Adaptive universal generalized pagerank graph neural network. *arXiv preprint arXiv:2006.07988*, 2020.

C Lee Giles, Kurt D Bollacker, and Steve Lawrence. Citeseer: An automatic citation indexing system. In *Proceedings of the third ACM conference on Digital libraries*, pp. 89–98, 1998.

Aditya Grover and Jure Leskovec. node2vec: Scalable feature learning for networks. In *Proceedings of the 22nd ACM SIGKDD International Conference on Knowledge Discovery and Data mining*, pp. 855–864, 2016.

Leo Katz. A new status index derived from sociometric analysis. *Psychometrika*, 18(1):39–43, 1953.

Thomas N Kipf and Max Welling. Semi-supervised classification with graph convolutional networks. *arXiv preprint arXiv:1609.02907*, 2016a.

Thomas N Kipf and Max Welling. Variational graph auto-encoders. *arXiv:1611.07308*, 2016b.

David Liben-Nowell and Jon Kleinberg. The link-prediction problem for social networks. *Journal of the American society for information science and technology*, 58(7):1019–1031, 2007.

Linyuan Lü and Tao Zhou. Link prediction in complex networks: A survey. *Physica A: statistical mechanics and its applications*, 390(6):1150–1170, 2011.

Linyuan Lü, Matúš Medo, Chi Ho Yeung, Yi-Cheng Zhang, Zi-Ke Zhang, and Tao Zhou. Recommender systems. *Physics Reports*, 519(1):1–49, 2012.

Costas Mavromatis and George Karypis. Graph infoclust: Leveraging cluster-level node information for unsupervised graph representation learning. *arXiv:2009.06946*, 2020.

Andrew Kachites McCallum, Kamal Nigam, Jason Rennie, and Kristie Seymore. Automating the construction of internet portals with machine learning. *Information Retrieval*, 3(2):127–163, 2000.

Miller McPherson, Lynn Smith-Lovin, and James M Cook. Birds of a feather: Homophily in social networks. *Annual review of sociology*, 27(1):415–444, 2001.

Ron Milo, Shalev Itzkovitz, Nadav Kashtan, Reuven Levitt, Shai Shen-Orr, Inbal Ayzenshtat, Michal Sheffer, and Uri Alon. Superfamilies of evolved and designed networks. *Science*, 303 (5663):1538–1542, 2004.

Galileo Namata, Ben London, Lise Getoor, and Bert Huang. Query-driven active surveying for collective classification. In *10th International Workshop on Mining and Learning with Graphs*, volume 8, pp. 1, 2012.

Mark EJ Newman. Finding community structure in networks using the eigenvectors of matrices. *Physical review E*, 74(3):036104, 2006.

Maximilian Nickel, Kevin Murphy, Volker Tresp, and Evgeniy Gabrilovich. A review of relational machine learning for knowledge graphs. *Proceedings of the IEEE*, 104(1):11–33, 2015.

Liming Pan, Tao Zhou, Linyuan Lü, and Chin-Kun Hu. Predicting missing links and identifying spurious links via likelihood analysis. *Scientific Reports*, 6(1):1–10, 2016.

Shirui Pan, Ruiqi Hu, Guodong Long, Jing Jiang, Lina Yao, and Chengqi Zhang. Adversarially regularized graph autoencoder for graph embedding. *arXiv:1802.04407*, 2018.

Hongbin Pei, Bingzhe Wei, Kevin Chen-Chuan Chang, Yu Lei, and Bo Yang. Geom-gcn: Geometric graph convolutional networks. *arXiv preprint arXiv:2002.05287*, 2020.

Yanjun Qi, Ziv Bar-Joseph, and Judith Klein-Seetharaman. Evaluation of different biological data and computational classification methods for use in protein interaction prediction. *Proteins: Structure, Function, and Bioinformatics*, 63(3):490–500, 2006.

Shai S Shen-Orr, Ron Milo, Shmoolik Mangan, and Uri Alon. Network motifs in the transcriptional regulation network of escherichia coli. *Nature genetics*, 31(1):64–68, 2002.

Nino Shervashidze, Pascal Schweitzer, Erik Jan Van Leeuwen, Kurt Mehlhorn, and Karsten M Borgwardt. Weisfeiler-lehman graph kernels. *Journal of Machine Learning Research*, 12(9), 2011.

Yunsheng Shi, Zhengjie Huang, Wenjin Wang, Hui Zhong, Shikun Feng, and Yu Sun. Masked label prediction: Unified message passing model for semi-supervised classification. *arXiv:2009.03509*, 2020.

Neil Spring, Ratul Mahajan, and David Wetherall. Measuring isp topologies with rocketfuel. *ACM SIGCOMM Computer Communication Review*, 32(4):133–145, 2002.

Zachary Stanfield, Mustafa Coşkun, and Mehmet Koyutürk. Drug response prediction as a link prediction problem. *Scientific Reports*, 7(1):1–13, 2017.

Lei Tang and Huan Liu. Leveraging social media networks for classification. *Data Mining and Knowledge Discovery*, 23(3):447–478, 2011.

Ashish Vaswani, Noam Shazeer, Niki Parmar, Jakob Uszkoreit, Llion Jones, Aidan N Gomez, Łukasz Kaiser, and Illia Polosukhin. Attention is all you need. In *Advances in neural information processing systems*, pp. 5998–6008, 2017.

Petar Veličković, Guillem Cucurull, Arantxa Casanova, Adriana Romero, Pietro Lio, and Yoshua Bengio. Graph attention networks. *arXiv:1710.10903*, 2017.

Christian Von Mering, Roland Krause, Berend Snel, Michael Cornell, Stephen G Oliver, Stanley Fields, and Peer Bork. Comparative assessment of large-scale data sets of protein–protein interactions. *Nature*, 417(6887):399–403, 2002.

Duncan J Watts and Steven H Strogatz. Collective dynamics of 'small-world'networks. *nature*, 393(6684):440–442, 1998.

Zonghan Wu, Shirui Pan, Fengwen Chen, Guodong Long, Chengqi Zhang, and S Yu Philip. A comprehensive survey on graph neural networks. *IEEE transactions on neural networks and learning systems*, 32(1):4–24, 2020.

Muhan Zhang and Yixin Chen. Weisfeiler-lehman neural machine for link prediction. In *Proceedings of the 23rd ACM SIGKDD International Conference on Knowledge Discovery and Data Mining*, pp. 575–583, 2017.

Muhan Zhang and Yixin Chen. Link prediction based on graph neural networks. *Advances in Neural Information Processing Systems*, 31:5165–5175, 2018.

Muhan Zhang, Zhicheng Cui, Shali Jiang, and Yixin Chen. Beyond link prediction: Predicting hyperlinks in adjacency space. In *Thirty-Second AAAI Conference on Artificial Intelligence*, 2018.

Muhan Zhang, Pan Li, Yinglong Xia, Kai Wang, and Long Jin. Revisiting graph neural networks for link prediction. *arXiv:2010.16103*, 2020.

Si Zhang, Hanghang Tong, Jiejun Xu, and Ross Maciejewski. Graph convolutional networks: a comprehensive review. *Computational Social Networks*, 6(1):1–23, 2019.

Appendix A. Ablation study

We conduct ablation studies of WalkPool by excluding or including only each of the node-, link- and graph-level features in (5). We used short notations $\{\texttt{node}^\tau\} \equiv \{\texttt{node}^{\tau,+}, \texttt{node}^{\tau,-} : \tau \in \{2, \cdots, \tau_c\}\}$, and similarly for $\{\texttt{link}^\tau\}$, $\{\Delta\texttt{graph}^\tau\}$. The ablation results for the C.ele dataset is shown in the In Table. 3.

Feature `feat`	ω_{12}	$\{\texttt{node}^\tau\}$	$\{\texttt{link}^\tau\}$	$\{\Delta\texttt{graph}^\tau\}$	-
AUC (using only `feat`)	87.90	91.88	92.44	92.29	-
AUC (using WP\`feat`)	92.69	92.66	91.08	92.65	92.82

Table 3: Ablation study in C.ele

Appendix B. Hyperparamters

The hyperparamters to reproduce the results are summarized in Table 4.

For the split of training, validation and testing edges, we have adopted different setups for datasets with and without node attributes to consist with previous studies. In particular, for datasets without node attributes, 90% of edges are taken as training positive edges and the remaining 10% are for testing positive edges. The corresponding same number of negative edges are sampled randomly for training and testing. Then among the training edges. we randomly selected 5% for validation. The observed graph from which the enclosing subgraphs are sampled consists of all the training positive edges. For the datasets with node attributes, all the edges are divided into 85% for training, 10% for testing and 5% for validation. The observed graph is built only based on the training edges. Some studies of link prediction choose to keep the observed graph connected when sampling the test edges, while others do not adopt this option. For the experiment results shown in the paper, we sample the test edges uniformly random without ensuring the observed graph is connected.

For sampling the enclosing subgraphs, we set the number of hops as 2 except 3 for the Power dataset. The 2-hop subgraphs sampled from E.coli and PB datasets and Pubmed are relatively numerous in nodes. Thus we set a maximum number nodes per hop for these two datasets to fit into memory. In particular, for each hop during sampling, we randomly select a maximum of 100 nodes if the sampled nodes exceeds.

For WalkPool, We set $\tau_c = 7$ for the cutoff of walk length in all experiments. When τ_c becomes large, the transition probabilities converges to a constant, as the random walk reaches stationary. Therefore, a larger value of τ introduces little further information. From experiments, we find that introducing a larger τ_c will not increase the accuracy notably.

For the classifer, we use a MLP with layer sizes $72 - 1440 - 1440 - 720 - 72 - 1$. We use Relu as the activation function for the hidden layers, and sigmoid function for the output layer.

Appendix C. Results measured by AP

The prediction accuracy measured by AP for datasets with and without node attributes are shown in Table 5 and Table 6, respectively. From the tables, WalkPool still performs best with the AP metric.

Appendix D. Locality of graph-level features

Let $G = (\mathcal{V}, \mathcal{E})$ be an enclosing subgraph, and $\{1, 2\}$ be the candidate link. We denote the random walk transition matrices on G^+ and G^- as $\mathbf{P}$ and $\mathbf{Q}$, respectively. For any node $x, y \in \mathcal{V}$, let $d(x, y)$ be the shortest path distance on the graph. We define the distance from x to the candidate link to be $\bar{d}(x) = \min\{d(x, 1), d(x, 2)\}$. We have the following result.

Name	With attributes	No attributes
optimizer	Adam	Adam
learning rate	5e-5	5e-5
weight decay	0	0
test ratio	0.1	0.1
validation ratio	0.05 of training edges	0.05 of all edges
batch size	32	32
epochs	50	50
hops of enclosing subgraph	(∗) 2	2
dimension of initial representation $\mathbf{Z}^{(0)}$	16	32
initial representation $\mathbf{Z}^{(0)}$	ones or DL	unsupervised models
hidden layers of GCN	32	32
output layers of GCN	32	32
hidden layers of attention MLP	32	32
output layers of attention MLP	32	32
walk length cutoff τ_c	7	7
heads	2	2

Table 4: Default hyperparameters for reproducing the reults. (∗): 3-hop for the Power dataset.

Data	**USAir**	**NS**	**PB**	**Yeast**	**C.ele**	**Power**	**Router**	**E.coli**
AA	95.36±1.00	94.46±0.93	92.36±0.46	89.53±0.63	86.46±1.43	58.76±0.89	56.50±0.51	96.05±0.25
Katz	94.07±1.18	95.05±1.08	93.07±0.46	95.23±0.39	85.93±1.69	79.82±0.91	64.52±0.81	94.83±0.30
PR	95.08±1.16	95.11±1.04	92.97±0.77	95.47±0.43	89.56±1.57	80.56±0.91	64.91±0.85	96.41±0.33
WLK	96.82±0.84	98.79±0.40	93.34±0.89	96.82±0.35	88.96±2.06	83.02±3.19	86.59±2.23	97.25±0.42
WLNM	95.95±1.13	98.81±0.49	92.69±0.64	96.40±0.38	85.08±2.05	87.16±0.77	93.53±1.09	97.50±0.23
N2V	89.71±2.97	94.28±0.91	84.79±1.03	94.90±0.38	83.12±1.90	81.49±0.86	68.66±1.49	90.87±1.48
SPC	78.07±2.92	90.83±2.16	86.57±0.61	94.63±0.56	62.07±2.40	91.00±0.58	73.53±1.47	96.08±0.37
SEAL	97.13±0.80	<u>99.06±0.37</u>	94.55±0.43	98.33±0.37	89.48±1.85	89.55±1.29	96.23±1.71	98.03±0.20
WP(ones)	<u>98.43±0.66</u>	99.04±0.28	<u>95.00±0.46</u>	<u>98.52±0.28</u>	<u>91.14±1.80</u>	<u>92.45±0.72</u>	<u>97.08±0.42</u>	<u>98.74±0.17</u>
WP(DL)	**98.66±0.55**	**99.09±0.29**	**95.28±0.41**	**98.64±0.28**	**91.53±1.33**	**93.07±0.69**	**97.20±0.38**	**98.79±0.21**

Table 5: Prediction accuracy measured by AP on eight datasets (90% observed links) without node attributes. Boldface letters are used to mark the best results while underlined letters indicate the second best results.

Proposition 1. *Let* $\mathcal{V}^\tau = \{x \in \mathcal{V}, \bar{d}(x) > \tau\}$*, then* $[\mathbf{P}^\tau]_{x,y} = [\mathbf{Q}^\tau]_{x,y}$ *for all* $x, y \in \mathcal{V}^\tau$*.*

Proof. We prove the result via induction. When $\tau = 1$, after the node-wise normalization from the softmax function in (2), the elements of $\mathbf{P}$ and $\mathbf{Q}$ are identical among nodes that not neighbors of the candidate link, i.e., $\mathcal{V}^1 = \{x \in \mathcal{V}, \bar{d}(x) > 1\}$.

Now suppose the claim holds for τ. Let $\mathcal{I} = \{x \in \mathcal{V}, \bar{d}(x) \leq \tau\}$, let $\partial\mathcal{I}$ be the set of nodes that are adjacency to but not in $\mathcal{I}$, and let $\mathcal{I}^c$ be the set of rest nodes in the graph. We can arrange the order of the nodes that such that $\mathbf{P}$ and $\mathbf{P}^\tau$ are of the following block form

$$\mathbf{P} = \begin{pmatrix} \mathbf{P}_{\mathcal{I},\mathcal{I}} & \mathbf{P}_{\mathcal{I},\partial\mathcal{I}} & \mathbf{0} \\ \mathbf{P}_{\partial\mathcal{I},\mathcal{I}} & \mathbf{P}_{\partial\mathcal{I},\partial\mathcal{I}} & \mathbf{P}_{\partial\mathcal{I},\mathcal{I}^c} \\ \mathbf{0} & \mathbf{P}_{\mathcal{I}^c,\partial\mathcal{I}} & \mathbf{P}_{\mathcal{I}^c,\mathcal{I}^c} \end{pmatrix}, \qquad \mathbf{P}^\tau = \begin{pmatrix} \mathbf{P}^\tau_{\mathcal{I},\mathcal{I}} & \mathbf{P}^\tau_{\mathcal{I},\partial\mathcal{I}} & \mathbf{P}^\tau_{\mathcal{I},\mathcal{I}^c} \\ \mathbf{P}^\tau_{\partial\mathcal{I},\mathcal{I}} & \mathbf{P}^\tau_{\partial\mathcal{I},\partial\mathcal{I}} & \mathbf{P}^\tau_{\partial\mathcal{I},\mathcal{I}^c} \\ \mathbf{P}^\tau_{\mathcal{I}^c,\mathcal{I}} & \mathbf{P}^\tau_{\mathcal{I}^c,\partial\mathcal{I}} & \mathbf{P}^\tau_{\mathcal{I}^c,\mathcal{I}^c}, \end{pmatrix} \tag{6}$$

where $\mathbf{P}_{\mathcal{I},\mathcal{I}}$ is the block matrix confined to $\mathcal{I}$ and other blocks are defined similarly. By definition, $\mathbf{P}_{\mathcal{I},\mathcal{I}^c} = \mathbf{0}$ and $\mathbf{P}_{\mathcal{I}^c,\mathcal{I}} = \mathbf{0}$. Multiplication of the block matrices gives

$$\mathbf{P}^{\tau+1}_{\mathcal{I}^c,\mathcal{I}^c} = \mathbf{P}_{\mathcal{I}^c,\partial\mathcal{I}}\mathbf{P}^\tau_{\partial\mathcal{I},\mathcal{I}^c} + \mathbf{P}_{\mathcal{I}^c,\mathcal{I}^c}\mathbf{P}^\tau_{\mathcal{I}^c,\mathcal{I}^c}. \tag{7}$$

	VGAE		ARGVA		GIC	
	NO WP	WP	NO WP	WP	NO WP	WP
Cora	92.65±0.59	95.11±0.53	93.11±1.08	95.23±0.84	93.45±0.48	**95.97±0.57**
Citeseer	92.28±0.92	94.89±0.89	92.69±0.85	95.04±1.46	95.11±0.65	**96.04±0.63**
Pubmed	96.60±0.13	98.46±0.14	96.52±0.20	98.49±0.14	92.32±0.37	**98.65±0.15**

Table 6: Prediction accuracy measured by AP on three datasets (90% observed links) with node attributes.

Data	**USAir**	**NS**	**PB**	**Yeast**	**C.ele**	**Power**	**Router**	**E.coli**
AA	88.61±0.40	77.13±0.75	87.06±0.17	82.63±0.27	73.37±0.80	53.38±0.22	52.94±0.28	87.66±0.56
Katz	88.91±0.51	82.30±0.93	91.25±0.22	88.87±0.28	79.99±0.59	57.34±0.51	54.39±0.38	89.81±0.46
PR	90.57±0.62	82.32±0.94	92.23±0.21	89.35±0.29	84.95±0.58	57.34±0.52	54.44±0.38	92.96±0.43
WLK	91.93±0.71	87.27±1.71	92.54±0.33	91.15±0.35	83.29±0.89	63.44±1.29	71.25±4.37	92.38±0.46
WLNM	91.42±0.95	87.61±1.63	90.93±0.23	92.22±0.32	75.72±1.33	64.09±0.76	86.10±0.52	92.81±0.30
N2V	84.63±1.58	80.29±1.20	79.29±0.67	90.18±0.17	75.53±1.23	55.40±0.84	62.45±0.81	84.73±0.81
SPC	65.42±3.41	79.63±1.34	78.06±1.00	89.73±0.28	47.30±0.91	56.51±0.94	53.87±1.33	92.00±0.50
SEAL	93.36±0.67	90.88±1.18	93.79±0.25	93.90±0.54	82.33±2.31	65.84±1.10	86.64±1.58	94.18±0.41
WP(ones)	95.16±0.70	90.68±1.04	94.50±0.20	94.89±0.22	**87.83±0.83**	67.03±0.77	88.09±0.52	**95.37±0.22**
WP(DL)	**95.50±0.74**	**90.97±0.96**	**94.57±0.16**	**95.00±0.21**	87.62±1.39	**67.72±0.86**	**88.13±0.61**	95.33±0.30

Table 7: Prediction accuracy measured by AUC on eight datasets (50% observed links) without node attributes. Boldface letters are used to mark the best results while underlined letters indicate the second best results.

Data	**USAir**	**NS**	**PB**	**Yeast**	**C.ele**	**Power**	**Router**	**E.coli**
AA	89.39±0.39	77.14±0.74	87.24±0.18	82.68±0.27	73.40±0.77	53.37±0.23	52.94±0.27	89.01±0.49
Katz	91.29±0.36	82.69±0.88	91.54±0.16	92.22±0.21	79.94±0.79	57.63±0.52	60.87±0.26	91.93±0.35
PR	91.93±0.50	82.73±0.90	91.92±0.25	92.54±0.23	84.15±0.86	57.61±0.56	61.01±0.30	94.68±0.28
WLK	93.34±0.51	89.97±1.02	92.34±0.34	93.55±0.46	83.20±0.90	63.97±1.81	75.49±3.43	94.51±0.32
WLNM	92.54±0.81	90.10±1.11	91.01±0.20	93.93±0.20	76.12±1.08	66.43±0.85	86.12±0.68	94.47±0.21
N2V	82.51±2.08	86.01±0.87	77.21±0.97	92.45±0.23	72.91±1.74	60.83±0.68	66.77±0.57	85.41±0.94
SPC	70.18±2.16	81.16±1.26	81.30±0.84	92.07±0.27	55.31±0.93	59.10±1.06	59.13±3.22	94.14±0.29
SEAL	94.15±0.54	92.21±0.97	93.42±0.19	95.32±0.38	81.99±2.18	65.28±1.25	87.79±1.71	95.67±0.24
WP(ones)	95.39±0.73	92.15±0.81	94.14±0.27	96.04±0.16	**86.49±0.97**	69.26±0.64	**89.21±0.44**	96.35±0.24
WP(DL)	**95.87±0.74**	**92.33±0.76**	**94.22±0.27**	**96.15±0.13**	86.25±1.42	**69.79±0.71**	89.17±0.55	**96.36±0.34**

Table 8: Prediction accuracy measured by AP on eight datasets (50% observed links) without node attributes. Boldface letters are used to mark the best results while underlined letters indicate the second best results.

We can do a similar computation to obtain $\mathbf{Q}^{\tau+1}_{\mathcal{I}^c,\mathcal{I}^c}$, with all $\mathbf{P}$ replaced by $\mathbb{Q}$ in the above equation. By assumption, we have

$$\mathbf{P}_{\mathcal{I}^c\partial\mathcal{I}} = \mathbf{Q}_{\mathcal{I}^c\partial\mathcal{I}} \qquad \mathbf{P}^{\tau}_{\partial\mathcal{I},\mathcal{I}^c} = \mathbf{Q}^{\tau}_{\partial\mathcal{I},\mathcal{I}^c} \qquad \mathbf{P}_{\mathcal{I}^c,\mathcal{I}^c} = \mathbf{Q}_{\mathcal{I}^c,\mathcal{I}^c}, \qquad \mathbf{P}^{\tau}_{\mathcal{I}^c,\mathcal{I}^c} = \mathbf{Q}^{\tau}_{\mathcal{I}^c,\mathcal{I}^c}, \tag{8}$$

as $\partial\mathcal{I}, \mathcal{I}^c \in \mathcal{V}^\tau$, therefore we obtain $\mathbf{P}^{\tau+1}_{\mathcal{I}^c,\mathcal{I}^c} = \mathbf{Q}^{\tau+1}_{\mathcal{I}^c,\mathcal{I}^c}$. As $\mathcal{I}^c = \mathcal{V}^{\tau+1}$, the claim follows by induction. □

Appendix E. Results with 50% observation

We further test of the performance of WalkPool under the setup of sparse training set. In particular, we keep only 50% positive links of the graphs for training and use the rest links for testing. The same number of negative links are sampled randomly for the traning set and test set. The results measure by AUC and AP are shown in Table 7 and 8, respectively.